70th International Astronautical Congress (IAC), Washington D.C., USA, 21-25 October 2019.

IAC–19–D1.6.6x54139

Towards Robotic On-Orbit Assembly of Large Space Telescopes: Mission Architectures, Concepts, and Analyses

Angadh Nanjangud[a,*], Craig I. Underwood[a], Christopher P. Bridges[a], Chakravarthini M. Saaj[b], Steve Eckersley[c], Sir Martin Sweeting[a,c], Paolo Bianco[d]

[a] *Surrey Space Centre, University of Surrey, Guildford, United Kingdom, GU2 7XH, a.nanjangud@surrey.ac.uk*
[b] *University of Lincoln, Lincolnshire, United Kingdom LN6 7TS*
[c] *Surrey Satellite Technology Limited, Guildford, United Kingdom, GU2 7YE*
[d] *Airbus, Anchorage Road, Portsmouth, United Kingdom, PO3 5PU*
[*] Corresponding Author

Abstract

Over the next two decades, unprecedented astronomy missions could be enabled by space telescopes larger than the James Webb Space Telescope. Commercially, large aperture space-based imaging systems will enable a new generation of Earth Observation missions for both science and surveillance programs. However, launching and operating such large telescopes in the extreme space environment poses practical challenges. One of the key design challenges is that very large mirrors (i.e. apertures larger than 3m) cannot be monolithically manufactured and, instead, a segmented design must be utilized to achieve primary mirror sizes of up to 100m. Even if such large primary mirrors could be made, it is impossible to stow them in the fairings of current and planned launch vehicles, e.g., SpaceX's Starship reportedly has a 9m fairing diameter. Though deployment of a segmented telescope via a folded-wing design (as done with the James Webb Space Telescope) is one approach to overcoming this volumetric challenge, it is considered unfeasible for large apertures such as the 25m telescope considered in this study. Parallel studies conducted by NASA indicate that robotic on-orbit assembly (OOA) of these observatories offers the possibility, surprisingly, of reduced cost and risk for smaller telescopes rather than deploying them from single launch vehicles but this is not proven. Thus, OOA of large aperture astronomical and Earth Observation telescopes is of particular interest to various space agencies and commercial entities. In a new partnership with Surrey Satellite Technology Limited and Airbus Defence and Space, the Surrey Space Centre is developing the capability for autonomous robotic OOA of large aperture segmented telescopes. This paper presents the concept of operation and mission analysis for OOA of a 25m aperture telescope operating in the visible waveband of the electromagnetic spectrum; telescopes of this size will be of much value as it would permit 1m spatial resolution of a location on Earth from geostationary orbit. Further, the conceptual evaluation of robotically assembling 2m and 5m telescopes will be addressed; these missions are envisaged as essential technology demonstration precursors to the 25m imaging system.

Keywords: on-orbit assembly, autonomous space robots, large aperture telescopes, small satellites, space systems engineering, mission concepts

1. Introduction

This study is about imaging "distant" objects at a high resolution using a large aperture telescope that is robotically constructed on-orbit and developing a staged approach to achieving such an end-game objective through a series of demonstration missions. Within the scope of this study, the definition of "distant" refers to the altitude of an Earth observation (EO) satellite located at Geostationary Earth Orbit (GEO) and the corresponding definition of "high resolution" is 1m for this telescope. The imaging system will operate in the visible waveband of the electromagnetic spectrum (λ = 0.4-0.75μm) and are thus also referred to as "optical" telescopes. This defines the "user requirement" for this study leading to the need for a 25m aperture primary mirror.

Systems such as the Hubble Space Telescope (HST) [1] and James Webb Space Telescope (JWST) [2] allow a reader to easily imagine what a space observatory could look like. Similarly, space robots such as the Space Station Remote Manipulator System (SSRMS) and Special Purpose Dexterous Manipulator (SPDM) of the International Space Station (ISS)'s Mobile Servicing Sys-

tem (MSS) [3] offer illustrations of a conceptual assembly robot. However, the vision of a robot assembling a space telescope is less straightforward to imagine. In this paper, a wide-ranging yet comprehensive discussion on optical space telescope design and their subsystems, a full mission architecture for robotically assembling a 25m aperture system, and a road-map eliciting mission concepts that would enable such robotic OOA with a single robotic manipulator, is presented. The robotic approach allows the volume and mass limitations to be overcome of current launch vehicles in achieving the on-orbit construction of large space structures. It also offers a significantly less complex approach to robotic assembly than other recent studies employing multi-limbed robots for assembly which requires more complex dual-arm manipulation and multi-legged locomotion [4]. In contrast, the design and architecture proposed here leverages space heritage design for a robot that is significantly more compact yet is uninhibited in its ability to relocate to different areas to perform assembly. A conceptual rendering of the assembly of a 25m aperture of a large telescope relevant to this study is shown in Figure 1.

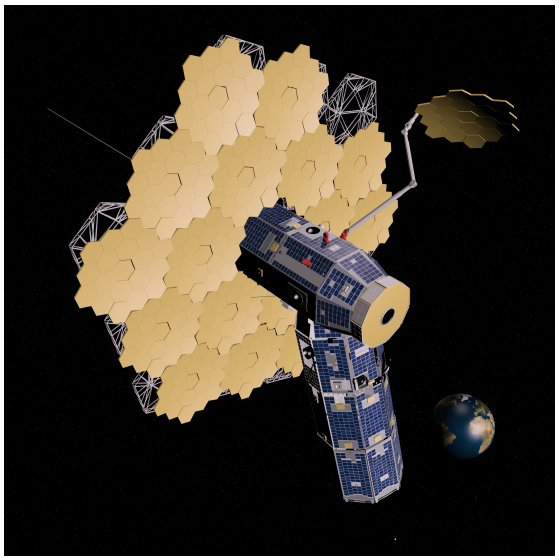

Fig. 1: Concept art depicting the assembly of a segmented primary mirror (PM) of a 25m space telescope by a robotic manipulator.

A space observatory assembled on-orbit by a robot principally comprises three fundamental systems:

- Optical Telescope Assembly (OTA) system,
- Robotic Agent for Space Telescope Assembly (RASTA) system, and
- Base spacecraft (s/c) system.

The focus of this paper is on translating the user requirements, defined above, into the requirements of the OTA. Requirements associated with the RASTA systems were presented in an earlier study [5], and are thus not presented here for sake of brevity. As robotic OOA is in its infancy, a clear preferred architecture is not easily identifiable within the space community; this permits a variety of conceptual ideas. With a baseline for the telescope design and robotic architecture, a mission architecture for assembling telescopes on-orbit is presented and analysed. In addition to aspects relating to the fundamental Concept of Operations (ConOps) for this end-game mission, three demonstration mission concepts are also proposed and analysed. The design of these missions is to systematically develop and demonstrate the technologies that will lead to the successful realization of the end-game mission of assembling a 25m space telescope in GEO.

2. Space Telescope Design

Broadly speaking, there are three categories of optical telescopes: refracting, reflecting, and catadioptric telescopes. As refractor telescopes suffer from chromatic aberrations at apertures over 1m, reflecting systems are common in space-based optical imaging. The introduction of corrector lenses into multi-mirror reflectors leads to the catadioptric imagers. This study limits its consideration to reflecting telescopes given their more prominent use in contemporary space-based astronomy. The next subsection presents a telescope design to meet certain user requirements; this is done by first converting said requirements into optical systems design requirements. Then, a qualitative discussion trading various reflecting telescopes leads to the selection of an apt telescope design and its subsystems-level design is further detailed.

2.1 Baseline optical system: from user requirements to optical system requirements

Here, the optical system requirements (i.e., the aperture size and the focal length of the imaging system) are calculated from from the user requirements: 1m spatial resolution from GEO ($36,000$km is assumed to be suitable as an approximation of the defined GEO altitude of $35,876$km) in the visible wavelength of the electromagnetic spectrum.

Aperture size: The aperture size of a telescope system is dependent on the wavelength at which observations are to be recorded and the desired angular resolution. First, the angular resolution (θ) is determined from the desired spatial resolution (r) and altitude of observation (h):

$$\theta = \frac{r}{h} = \frac{1 \text{ m}}{36,000\text{km}} = 2.78 \times 10^{-8} \text{ radians} \quad [1]$$

Then, for the mid-band wavelength of the visible spectrum (λ= 0.55μm), the aperture size (D) is obtained from the Rayleigh criteria:

$$D = 1.22\frac{\lambda}{\theta} = 24.13 \text{ m} \quad [2]$$

Thus, a 25m diameter primary mirror (PM) is chosen, which would give a slightly larger light collecting area than the diameter above. Indeed, for diffraction limited performance at the red-end of the visible spectrum (λ= 0.70μm), the necessary diameter is $\sim$30 m; however, in keeping with Surrey Satellite Technology Limited (SSTL)'s user requirements as stated in [6], the telescope will be diffraction limited at 0.55μm.

Focal length: For the given user requirement of 1m resolution in the optical wavelength from GEO, an appropriate detector must be selected and located at the image plane to determine the focal length of the telescope, which is a significant driver of the choice of telescope design. To this end, the Focal Plane Assembly (FPA) is assumed to consist of a grid of complementary metal-oxide-semiconductor (CMOS) detectors; the assumed CMOS sensor for the calculations presented here is based on the Teledyne-E2V Emerald 16M [7]. We assume each detector has 4096 $\times$ 4096 pixels, (i.e., 16 megapixels) and each pixel is a square of side 1.4 μm. The effective focal length, f, should give sufficient magnification for one pixel to be equivalent to 1m on the ground from GEO and is given by:

$$\frac{f}{h} = \frac{x}{r} \quad [3]$$

where,

h, altitude of telescope = 36,000km,

x, pixel cell size = 1.4 μm, and

r, distance to be resolved = 1 m;

leading to f = 50.4m. In other words, achieving a 1m ground spatial resolution with a Newtonian focus could require a physical truss structure to provide up to 50.4m of separation between the PM and the FPA. Achieving this separation distance for optical imaging is an unprecedented challenge for space structures but one that will be necessary for long focal length space telescopes with ultra large apertures. The largest comparable such structure with flight heritage was the deployable mast used on the Shuttle-based Shuttle Radar Topography Mission (SRTM). This mast linearly deployed radar instruments to 60m from the mast mount point of the Space Shuttle; at radio wavelengths, large deployment errors (i.e., at millimetre-level) are permissible. However, accurate measurements in the "visible" domain require nanometre-level deployment precision of structures. This is yet to be achieved in space and is recognized as one of the key enablers for visible imaging with large apertures [8]. Further, the structure must remain rigid in its deployed state to ensure that alignment between the FPA and PM is maintained at errors of the order of tens of nanometres [8]. As such precision is not yet achievable through structures alone, a precision control subsystem comprising actuators and wavefront sensors will need to be employed. Thus, the choice of telescope design is primarily driven by this focal length.

Reflecting telescopes in which the eyepiece is replaced by a FPA comprising various imaging sensors are also referred to as prime focus telescopes. Prime focus designs are common in astrophotography and essential to any space telescope. Based on the location of the focal plane in relation to the PM and/or number of mirrors used, they can be classified in three categories. A Newtonian focus is one where there is no secondary optics; the image is formed at the focal point of the PM. A Cassegrain focus is one which uses a folded-optical design with two mirrors and the focus lies behind the PM. The classic Cassegrain configuration uses a parabolic reflector as the primary while the secondary mirror (SM) is hyperbolic. Some of its other variants are discussed below:

1. **Ritchey-Chrétien (R-C) design**: In a R-C variant of such a telescope, both mirrors are hyperbolic. It is designed to eliminate spherical aberrations and coma but suffers from off-axis astigmatism. It is the most commonly used design in large professional-grade research telescopes. Notably, the HST is a Cassegrain design.

2. **Schmidt-Cassegrain design**: This is a catadioptric version of Cassegrain; it uses a spherical PM and a Schmidt corrector plate (an aspheric lens) to correct for the spherical aberration. This design is commonly used by telescope manufacturers as they are compact and use simple spherical optics. This design was also used on the Kepler space telescope used for exoplanet detection.

3. **Maksutov–Cassegrain** design: This is another catadioptric Cassegrain design, with spherical mirrors. It uses a full-aperture spherical meniscus corrector lens, which is easier to manufacture than the Schmidt plate, to eliminate coma, and aberrations (spherical and chromatic). Lastly,

three-mirror anastigmat designs use three curved mirrors to minimize spherical aberration, coma, and astigmatism. These are used to enable wide fields of view, much larger than possible with telescopes with just one or two curved surfaces. A variant of this design, called the Korsch telescope, is being used in the JWST. The increase in number of mirrors makes the overall alignment issue significantly more complex.

The structural challenges posed by large focal length and aperture telescopes, such as that seen with the end-game telescope, can only be overcome by using a telescope design that 'folds' the optics by using multiple mirrors, i.e., one of the Cassegrain focus designs. As highlighted earlier, the ∼50m separation for Newtonian designs is an unprecedented challenge for optical space telescopes. The Cassegrain system's folded optics allows uses a more compact geometric design without compromising the necessary overall (or effective) focal length for a GEO space telescope with 1m spatial resolution. Thus, of the two broad categories of reflecting telescopes, a Cassegrain is considered the most feasible option. As discussed above, the Cassegrain telescope has several variants, each of which have their own benefits. The R-C telescope design uses hyperbolic mirrors for both its primary and secondary mirrors whereas the classical Cassegrain uses a parabolic PM. This design is free of coma and spherical aberration, making it well suited for wide field and photographic observations. It is commonly used in large professional research telescopes, including the HST. The catadioptric variants are also compelling options as they use spherical mirrors that are cheaper and easier to manufacture. However, they pose a major challenges for the end-game telescope as the corrector lens, which is of nearly the same size as the PM, will thus also require OOA. The three-mirror option will require stringent alignment requirements for optical imaging that significantly drive up the control complexity and is thus also considered inappropriate for the end-game telescope, at this point. Thus, the R-C design is chosen for the telescope which is further detailed using equations and the schematic shown in Fig. 2 provided by Lockwood Optics [9] using the following parameters:

- PM and SM diameters are $D1$ and $D2$,
- focal length of the primary is $f1$,
- primary-secondary separation is d,
- system focal point to secondary distance is q,
- PM surface to focal plane distance is e, and
- distance from SM to focal point of PM is p.

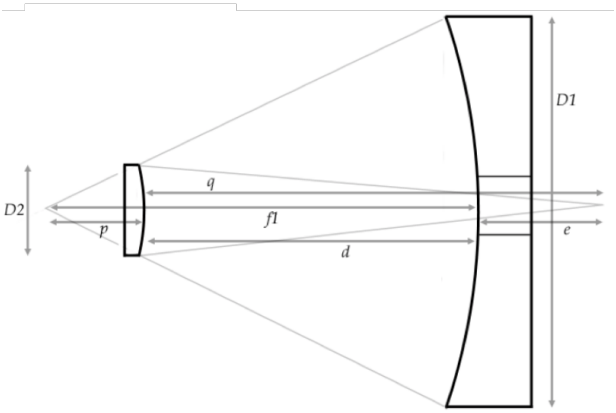

Fig. 2: R-C telescope schematic [9]

Additionally, the magnification of an R-C telescope is defined as $M \triangleq q/p$; it is a dimensionless parameter. M also encodes in it information regarding how much the effective focal length can be folded relative to that of the PM; M can be range from 3 to 15 for any Cassegrain configuration.

Given $D1$, $D2$, M, and the system's effective focal length, f, the goal is to determine p, q, e, d, and $f1$. Note that $D1$ and f were already determined as 25m and 50.4m, respectively, to meet SSTL's aforementioned user requirements. $D2$=2.4m is assumed; the rationale here is that it is feasible to manufacture a space-grade monolithic mirror of this size (e.g., HST). Lastly, $M = 10$ is assumed in the calculations. The central opening in the PM is assumed to be ∼5.5m in the case of the proposed large aperture telescope on account of its assembly around a central hub spacecraft. Thus, regardless of the separation between the two mirrors, the 2.4m SM will not block any of the light collecting area of the PM. For this telescope system, the PM's focal length is

$$f1 = \frac{f}{M} = 5.04\text{m}. \quad [4]$$

The distance between SM and PM's focal point is:

$$p = \frac{D2}{D1} f1 = 0.48 \text{ m}. \quad [5]$$

The separation between the primary and secondary mirrors is determined by first calculating

$$q = \frac{M}{p} = 4.84\text{m}. \quad [6]$$

and the distance from the primary to the focal plane:

$$e = p(M+1) - f1 = 0.28\text{m}. \quad [7]$$

Then the separation distance, d=4.56m, between the mirrors for the R-C telescope is determined which is seen to be remarkably lesser than that for the Newtonian design, asserting the superiority of the two-mirror design for large focal length telescopes. Assuming reasonable improvements in the current state-of-the-art in deployable systems, formation flying of the secondary can also be avoided for folded telescope designs at a 25m aperture, as indicated here. In the proposed telescope system, deployable masts will permit the positioning of the SM. In the next section, the full OTA is studied from a systems perspective and an initial technology assessment is performed for its various subsystems.

2.2 Optical Telescope Assembly: Technology considerations

A R-C OTA comprises four main structural elements: (i) segmented primary mirror assembly (PMA), (ii) modular backplane structure (supports the PMA), (iii) deployable SM with baffles, and (iv) FPA with baffles. Each of these are discussed in further detail below and the sizing of this OTA is summarized in Table 5.

2.2.1 Segmented PMA

Building a gigantic telescope from a monolithic mirror presents many challenges, which typically grow rapidly with the increasing size, and quickly make monolithic mirrors impractical. Some key issues are [10]: reduced availability of mirror blank material; passive support of mirror results in large optical deflections; very expensive mirror produces high risk of breakage from mishandling; larger mirrors are subject to larger deformations from thermal changes; vacuum chamber for mirror coatings becomes very large and expensive; tool costs for all parts (fabrication and handling) are large; shipping is difficult; and large space-based telescopes are crippled by limitations imposed by launch vehicles' fairing size. Thus, robotically assembling a large PM from smaller segmented mirrors is garnering significant attention both for earth-based and space-based astronomy. The advantage of smaller segments is that they are easier to fabricate, transport, install, and maintain than large monolithic mirrors. However, there are several challenges associated with segmented mirrors relating to their manufacturing, performance, and their sizing/packing for robotic OOA. These are discussed below.

2.2.1.1 Mirror Manufacturing Technologies

In telescopes, a mirror substrate serves two purposes: it supports the thin reflective coating (approximately a few hundred atoms thick) and provides structural support. At geostationary orbit, the telescope is exposed to both to the heat of the Sun and the intense cold of space; for this purpose, silver and aluminium are both options as mirror coatings for observations in the visible and infrared (IR) wavelengths. As aluminium does not tarnish as easily on the ground as silver, it is likely the better candidate for mirror coating [11] and was also used for this purpose on HST. For ground telescopes, glass is commonly used for the substrate. Mirrors on space telescopes require different properties such as having a low coefficient of thermal expansion (CTE) and being lightweight. Thus, silicon carbide (SiC), Ultra-Low Expansion® glass (ULE), beryllium (Be), carbon fibre reinforced plastic (CFRP), and ZERODUR have been considered as substrate material choices for space telescopes. Each of these materials is discussed in further detail below, based on discussions presented in [8] and [12], to identify a suitable mirror material for the end-game telescope system.

CFRP has the lowest contraction ratio when the temperature drops from room temperature to the operational temperatures (-100^{o}C to 125^{o}C for exposed mirrors and solar panels [13]) in space and segments up to 1.5m have been manufactured. However, CFRP segments are yet to meet the tight surface requirements for space observatories (which is one among several reasons why beryllium was preferred in the JWST [14] after more than two decades of development. Thus, it is not considered as a candidate for the end-game telescope in this study.

SiC is a potential mirror substrate candidate for the end-game telescope. SiC is an attractive material because it is inexpensive to produce, and it can be easily formed into unconventional shapes. SiC's biggest advantage is its very high specific stiffness. Specific stiffness is defined as E/ρ, where E is Young's modulus and ρ is the mass density. Ideally, lightweight mirrors should be constructed from something that has a large E (takes lots of stress with little strain) and a low density (lightweight for its size).

SiC presents several challenges, as well. First, the material is very hard, and this makes the polishing effort difficult and time-consuming. According to [12], no SiC parts have been fabricated at scales larger than 0.5 meter presenting a significant hurdle to overcome for their use on larger aperture telescopes. SiC also faces challenges becoming accepted into the space mirror community because it lacks the successful legacy of ULE and Be. There are currently few funded projects that use a SiC mirror [15, 16, 17]. Lastly, because so few mirrors have been created, the long-term stability of these materials for mirrors is unknown.

ZERODUR is a glass/ceramic mirror substrate material, manufactured by Schott, that has a very low CTE. They were thus considered as an option for space telescopes and have been tested for a deep space mission

(Deep Impact)[18]. They remained at or below 0.035 of the root mean square (RMS) figure over the 170 K cool-down from room to operational temperatures in deep space for the mission, indicating its suitability for the GEO telescope. The US Air Force Large Active Mirror Project has demonstrated a 4m actively controlled segmented PM operating in a vacuum environment (although at 300K); this mirror has an areal density of 140kg/m^2. This makes ZERODUR® an option for the GEO end-game large aperture telescope at this time but it is not a lightweight option.

ULE has been used for the mirrors on the HST and Kepler telescope. The HST mirrors have an areal density of 180kg/m^2 making it approximately ten times heavier than the beryllium mirrors on the JWST. However, a new generation of ULE was recently studied at the University of Arizona[12]; the resulting substrate material prototype had an areal density of 21kg/m^2. Glass has generally been the legacy material for mirror substrates as it is thermally stable; it can be engineered into a stiff structure with minimal residual stress; and the face sheet can be polished to a high-quality optical surface.

This makes ULE a highly attractive choice as the mirror substrate material for the end-game telescope. The sizes of substrates manufactured for University of Arizona, by Composite Optics (acquired by ATK) in San Diego, range in size from 0.5m to 2m. Interestingly, the areal density of the 2m mirror is 13kg/m^2; it was manufactured as part of mirror technology studies for the JWST. The costs for these mirrors were not published but it is important to note that areal densities may further be reduced for glass as the related manufacturing technologies mature. This makes it a more viable option than Be which is difficult to mine (and thus more expensive) and toxic.

Be is a particularly desirable material for mirrors as it has a low areal density of 20kg/m^2. In comparison to the low areal density ULE studied in [12], fewer actuators are necessary because Be is much stiffer than glass; it is five times stiffer than ULE and six times greater than aluminum. Be's biggest advantage as a mirror substrate is its high specific stiffness. Verbatim from [12]: "Beryllium is one of the stiffest, lightest materials that mirror-making money can buy." It has a near-zero CTE when used below 100 K which makes it an ideal material for cryogenic mirrors. This combination of properties makes Be a suitable candidate for the end-game telescope's mirrors.

However, it also has some important disadvantages. Firstly, its stiffness makes it very time-consuming to polish. Be also has a very low yield stress and cannot be stressed much before it does not spring back to its initial shape. Also, the particulate form of Be is toxic, so it must be polished and tested in special, controlled environments; this drives up manufacturing costs. Finally, there is not the established legacy for Be as there is for ULE (which will change once the JWST launches). As such, few manufacturers have the tooling and experience needed to successfully polish Be. All of these factors mean that Be is several times more expensive to work with than ULE.

Ideal GEO telescope mirrors were also briefly discussed in [12], which states that the Earth-imaging community has determined that a successful mirror for persistent imaging from GEO must have an areal density of 5kg/m^2. However, more recent discussions indicate that while areal density is a critical criterion for mirror material selection, it is not the sole criteria as there are threshold values for it at which mirrors do not survive launch loads; in other words, reducing the areal density reduces mirror stiffness that leads to its failure at launch. For this reason, JWST mirrors had their areal densities increased from 18kg/m^2 to 28 kg/m^2 [8].

So, from this discussion it is apparent that there are two key characteristics that are taken into consideration when selecting mirror materials for space telescopes: their stiffness and areal density. Low areal density result in low mass, offering two options from the above list of choices: the new generation of ULE and Be, both of which have an estimated areal density of 20kg/m^2, which can be sufficiently increased for the mirrors to survive launch loads.

However, as discussed above, these materials do not have comparable stiffness; Be is five times stiffer and has a low CTE. Also, Be requires fewer actuators than ULE. This increase in actuation also provides more control authority for maintaining a mirror's surface figure (which is why glass mirrors are sometimes referred to as high-authority mirrors [12]), which is important for EO systems. [8] speculates that, in contrast to astronomical observatories, an EO system may require a mirror with high authority control due to the mechanical and thermal dynamics of the chosen orbit. As telescopes operating in Low Earth Orbit (LEO) are prone to more thermal cycling than a telescope at GEO, ULE might be more appropriate for the former class of EO systems whereas Be is likely be better suited in the latter case. However, a conclusive statement on the level of authority required at LEO and GEO can only be determined via practical testing on the ground in thermal vacuum chambers. For the mission analyses in this study, the state-of-the-art indicates that areal densities of 20kg/m^2 are achievable with either Be or ULE, which is what is assumed for all the missions defined herein unless otherwise stated. As the Be substrate possesses superior areal density leading to lightweight mirrors without compromising stiffness, its use is assumed in all of the telescope missions analyzed

here; this is also because Be will soon be space-qualified on the JWST whereas the lightweight ULE is yet to be qualified. However, attention must continue to be paid to the progress made on this new generation of glass as it offers several benefits when compared to Be such as ease of manufacturing and its non-toxicity; ultimately, it is likely that both mirror technologies will be necessary depending on the orbit of operation for EO and their respective advantages.

2.2.1.2 Wavefront Sensing and Control

For a segmented PMA in a telescope to deliver an image quality comparable to that of a monolithic one, the segments need to be [19]: co-aligned (stack the images produced by each segment), co-focused (ensure that focal length of each segments is the same), and co-phased (no 'piston' discontinuity between the edges of neighbouring segments). A detailed discussion on the effects of segmentation, and in particular the effect of piston errors on the point spread function (PSF) of a segmented telescope, are discussed in Chapter 2 of [20]. The image quality of a segmented telescope will be affected by segment misalignment errors of the PM; achieving optical performance comparable to a monolithic PM requires phasing of segments to an accuracy that is a fraction of the observed wavelength. In the case of segmented optical telescopes, precision in error sensing is of the order of tens of nanometres ($\lambda/14$) and nanometre-level motion control is needed for the alignment of each mirror segment [12]. The subsystem responsible for achieving this perfect mirror alignment is known as the wavefront sensing and control (WFSC) subsystem; its objective is to reduce the wavefront error and is thus one of the most crucial subsystems of an operational telescope. Wavefront and phasing sensors are used to detect wavefront error which is related to piston errors (a measure of position error of the mirror). The wavefront errors are fed into the control system that computes appropriate actuation commands to achieve the required alignment of the mirror by reducing piston errors.

Wavefront and edge sensors: The basic requirement of wavefront sensors is to detect the wavefront error with enough sensitivity; diffraction limited imaging is achieved at wavefront RMS errors that are less than $\lambda/14$, which gives a Strehl ratio of 0.8 [20]. The Shack-Hartmann sensor is one such wavefront sensor that reaches an accuracy of about $\lambda/40$; a reference light source within the Shack-Hartmann sensor generates a reference wavefront which is used to provide an error measurement to the control system.The Shack-Hartman sensors have been successfully used for the phasing of the Keck telescopes and will also be used in the Autonomous Assembly of a Reconfigurable Space Telescope (AAReST) mission (only for focusing). The Zernike Phase Contrast Sensor is an alternative phasing sensor [20], which was found to be more precise than the Shack-Hartmann sensor. Both sensors will be located on the FPA, along with the detectors; while a detailed design of the FPA is out of the scope of this work, the authors assume that the wavefront sensors could be placed within the imaging array.

In addition to phasing sensors, the WFSC subsystem will also utilize edge sensors that are attached to every mirror to measure relative displacements between segments. A control loop between these edge sensors and position actuators allows accurate positioning of mirrors; the edge sensors may drift and might themselves need periodic calibration, which is where the use of the aforementioned phasing sensors is needed in segmented telescopes. The edge sensors on the Keck telescopes are made of low-expansion ceramic glass and have an operating range of $+/-20\mu$m [20]. Apart from periodically re-calibrating edge sensors, these phasing sensors will also aid servicing aspects of segmented space telescopes as they provide the zero reference for edge sensors on newly integrated segments that might be part of a future servicing mission.

Position and curvature control: There are two aspects for position control of mirror segments for appropriate optical performance: position control of the segment's rigid body degrees-of-freedom (DoF) and its curvature control. Of the six rigid body DoF per segment, the two lateral translations and the in-plane rotation have much smaller impact on wavefront error and thus, position control typically addresses the three out-of-plane DoF:

- 'piston' degree-of-freedom, which is the translation along the axis perpendicular to the segment,
- 'tip', and 'tilt' degrees-of-freedom, which are rotational degree-of-freedom about two axes in the horizontal plane of the segment.

Mechanical actuators move each segment in these three rigid body DoF; this mirror actuation necessary to generate the appropriate overall PM surface is commonly referred to as 'active optics'. In the JWST, six actuators are used to provide redundancies in the event of a failure of one of the actuators [21]; the design of the actuators is based on a Stewart platform (also referred to as a 3-6 hexapod), where each actuator has a minimum step size $<$10nm and a range $>$17.5mm [22]. Thus, it is apparent that candidate space-qualified actuators already exist for this precision motion technology; the European-Extremely Large Telescope, which has 798 hexagonal segments in its 39m PM, will make use of piezo and voice-coil-based actuators manufactured by PI-USA which provides the required step size ($\sim$1.7nm) for imaging in the optical wavelength [23].

To further ensure optical stability, mirror surfaces should accurately align to the prescribed curvature of the parent mirror. One approach that is currently being proposed to facilitate this is by using deformable mirrors, which carry piezoelectric actuators on their surface; this approach, also referred to as 'adaptive optics', will soon be demonstrated in the AAReST mission. In contrast, the JWST uses an actuator subsystem for the tip/tilt/piston motion control for co-phasing and a radius of curvature actuator for shape control of each mirror segment; the latter is a strut-based flexure system that self-balances to assure the uniform loads are applied at six outer points of the mirror. The actuator is attached between the confluence of the rods and the segment centre such that the centre of the mirror may be pushed or pulled in reaction to the vertices to make small changes in the mirror radius of curvature. This allows the curvature of all eighteen mirrors to be matched to achieve the necessary optical performance. For the end-game telescope, these flexures might need in-house development or, if the deformable mirrors approach is desired, collaborations with the AAReST team (Surrey Space Centre (SSC) and California Institute of Technology (CalTech)) could be sought. The choice of technology will ultimately depend more on the optical performance in the visible spectrum (i.e. wavefront RMS errors less than $\lambda/14$) and on space heritage.

In summary, the challenges of the WFSC are both in the high precision sensing and actuation necessary; given the current positive progress on both aspects, the precision required here for space-based optical imaging are not considered insurmountable challenges but definitely significant ones [8].

2.2.1.3 PMA Sizing

From the preceding discussion on mirror materials, the PMA sizing and costs can be determined; the PMA is the main driver for the mission mass as all other structures are monolithic (rigid and/or deployable) and are assumed to be of fairly constant mass. Also, it is the segmentation of the PM that leads to multiple launches, another major cost driver. Be is the chosen mirror substrate material for the end-game telescope, which has an assumed areal density of 20kg/m^2. From this, an optimal mirror size can be identified for the telescope from the data presented in Table 1. The areal cost for each mirror is assumed to be \$6 million/m^2 based on extant work on JWST [8]; it is interesting to note that the areal cost for Be mirrors used in JWST is half that for HST's ULE mirrors. It should also be noted that, for the JWST these numbers may have increased by an order of magnitude on account of the delays but, as yet, no reference can be found to ascertain this. However, these numbers are sufficient to make a decision for mirror segment size across a single substrate material.

Segment size (m)	**Number of segments**	**Mass (kg)**	**PMA cost ($Bn)**
1	342	5923	1.77
0.5	1368	5923	1.77
0.3	4104	6402	1.92
0.2	8892	6224	1.86
0.1	34200	5814	1.78

Table 1: 25m PMA comparison: segment sizes, mass, and costs.

Though the PMA made from 0.1m mirrors is lighter than one made from larger segments of 0.5m and 1m segments, it is also more expensive; thus, the 0.1m segment is considered to be unsuitable for the 25m end-game telescope given its higher cost and complexity of the WFSC. There are no apparent trade-offs with respect to cost and mass between 0.5m and 1m segments; the 1m segment is chosen given that it needs significantly fewer actuators for WFSC and that there is the possibility of manufacturing lighter mirrors at larger sizes based on the work presented in [12]. In other words, an apt segment is chosen based on the simplicity in operating the telescope and potential for mass reduction. Also, as the mirror segments get larger than 1m, every mirror cannot be identical in surface shape to conform to the larger aperture that the mirrors must conform to; it is for this reason that the JWST employs identical 1.3m segments, which appears to be the limit at which identical mirrors can be used for larger aperture telescopes. Thus, the 25m aperture PMA is made up of 342 segments of 1m hexagonal segments, flat-to-flat. Note that the effect of the reduced fill-factor is a reduction in the image brightness, which is captured by a parameter called '*f*-number' or 'focal ratio'; *f*-number is the ratio of focal length to diameter and a value under 11 is believed to be acceptable for a bright image. For the various segmented designs proposed here, the *f*-number is found to be between 5 and 5.2; for a filled aperture system, the *f*-number is $\sim$4.

Cost estimation is a fairly active field of research but one driven mostly by the JWST team who have developed a variety of parametric cost estimation models [24, 25, 26]; the areal cost assumed in this report is also derived from their work [8]. Estimating costs for large space telescopes is especially difficult given the limited data points of such systems and the lack of segmented systems only makes this estimation more challenging. The most interesting of their research findings is that while duplication of segments reduces the cost of manufacturing

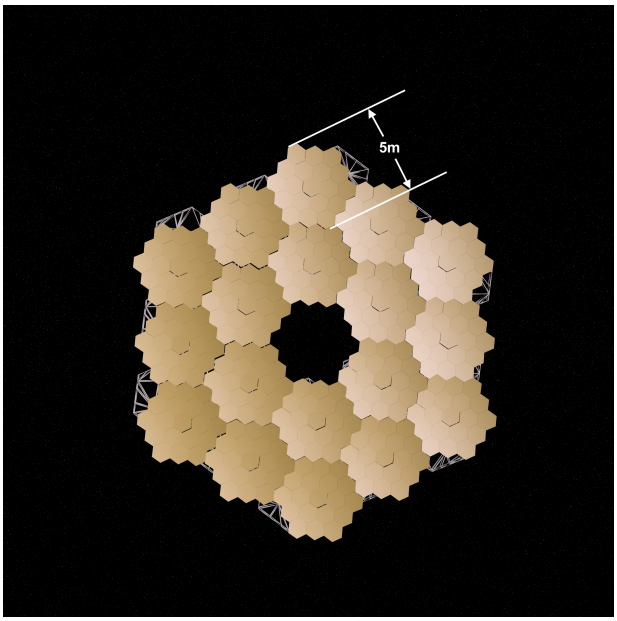

Fig. 3: Final arrangement of 18 mirror modules that make up the PMA.

mirrors of segmented PM over that of a monolithic mirror, the savings does not appear to manifest itself in the final PMA. They speculate that this is due to the increase complexity in the structure for supporting a segmented PM.

To minimize the overall number of pick-and-place operations performed by the robot, the PM is divided into 18 mirror modules and each module further comprises 19 hexagonal mirror segments (1m flat-to-flat). The full PMA is shown and the dimensions of an individual module is indicated in Fig. 3.

In addition to robotic assembly complexity, the launch vehicle faring size also drives the design of the mirror module. Of particular importance is the internal diameter of the fairing. No extant launcher can accommodate monolithic non-deployable spacecraft in excess of ∼4.5m. Thus, several upcoming launch vehicles were surveyed of which two were considered for trade-off evaluation: the Ariane 64 and the New Glenn.

In the selection of the appropriate mirror module design and launch vehicle, the following requirements were identified: the combination of module design and launch vehicle must minimize the number of robotic pick-and-place operations; the launch vehicle fairing must be wide enough to ensure that the mirror module shall not require a deployable systems philosophy (such as winged deployables used on the JWST); and the fairing should provide the volume to accommodate a spacecraft bus within which the mirror modules are stowed.

Two design options of the mirror module are considered: the first is as design shown in Fig. 3 where each module comprises 19 hexagonal segments. In this option, the segments with the precision actuators are mounted on a lightweight rigid backplate that will itself interface with the backplane deployable perimeter truss modules (DPTM). This design slightly exceeds the internal diameter of the Ariane 64, which is 4.57m. A fragmentation of this module's design that could fit within the Ariane 64 is shown in Fig. 4; here, each coloured set represents a submodule that, when assembled, would give the overall configuration of the 19 mirror module. Here, the central module (yellow) is the largest with flat-to-flat length of 3m. This design is considered as the backup option for the proposed mission if the Ariane launcher is used.

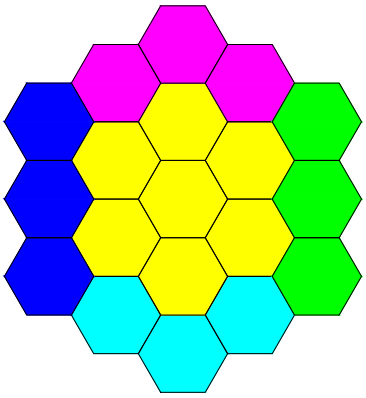

Fig. 4: Fractionated mirror module design for Ariane launcher.

Though design option 2 satisfied requirements 2 and 3, it violates requirement 1; the full assembly of the 25m telescope's PM portion (without backplane) would require nintey pick-and-place motions with option 2, whereas it would require only eighteen such motions using option 1. Innovative designs for each mirror module can also be explored, such as those discussed by Feinberg et al [27], but unless each module can accommodate more mirror segments, the requirements identified above would not be fully met.

The New Glenn, which has a 6.2m fairing, is thus the chosen launch vehicle. National Aeronautics and Space Administration (NASA)'s Space Launch System (SLS), which will have an internal fairing diameter of ∼8m, would be a good candidate but will certainly be significantly costlier (likely to be an order of magnitude higher). It also is not likely to have the same launch frequency, which could severely constrain the mission planning flexibility. The payload-to-GTO capacity of the New Glenn is 13 metric tons.

Table 2 summarises the properties of the mirror mod-

ule; in addition to the mass of 19 mirrors, each module mass also includes additional 80% of segment mass as margin towards the actuator and the lightweight rigid backplate.

Parameter	Quantifier
Number of 1m segments per module	19
Module mass (kg)	592kg

Table 2: Mirror module sizing summary.

2.2.2 Modular Backplane

Assembling the backplane to accommodate the geometry of the PM surface presents the next structural challenge for the 25m end-game telescope. The requirements here are that: the structural elements must stow compactly in the launch vehicle; the full backplane must be assembled using a single manipulator; and the full backplane structure must remain adequately stiff and thermally stable to satisfy the precision optical imaging requirements.

To satisfy the first requirement, a modular backplane assembled from deployable perimeter trusses was chosen. Ref. [4] identifies a hexagonal PacTruss configuration [28] to be most compatible with hexagonal mirror segment geometry and thus it was the chosen DPTM design. Note that a backplane structure could also be assembled using struts and nodes, as opposed to DPTMs; for instance, robotic assembly of a truss structure, comprising 102 struts, has been demonstrated which was reported to have taken roughly 20 hours [29]. In contrast to this approach, deployable trusses would greatly reduce the number of operations in creating the backplane and are thus a more efficient approach to orbital assembly of backplanes. Constructing with struts and nodes would also require more than one manipulator, violating the third requirement. It is also an antithesis to the low cost, mass, and complexity mission objectives of this study.

The DPTM-based approach to constructing the backplane assembly relies on a combination of assembly and deployment. Two approaches were considered towards constructing the backplane from DPTMs:

1. auto-deployment after attachment to the PM hub (in essence, this is the spacecraft bus) via a connector interface, or

2. using the robot for deployment of the truss and placement at the connector interface to the hub.

Though, either approach avoids reliance on pure deployment or pure assembly of the backplane, the use of DPTMs is preferred to enable a low-mass, cost, and power single manipulator architecture, thus satisfying requirement 2. Pure deployment of the supporting backplane structure alone would also require numerous mechanisms for a large structure and present substantial mechanical challenges; e.g., mechanism actuation without jamming for large scale deployment. Ground-based testing of such large single deployable systems (i.e. one deployable backplane for the 25m telescope) is also challenging when compared to that of smaller modules.

The DPTMs will be designed to deploy like the AstroMesh ring trusses [30]. This technology has been demonstrated in space on various missions, e.g., in Soil Moisture Active Passive (SMAP) where a flexible mesh antenna was deployed (using such a perimeter truss) from a stowed diameter of 0.3m to deployed diameter of 6m. Deployed surface precision of 0.3mm RMS error for a 9m diameter antenna has been demonstrated, which is presumed to be acceptable for the modular backplane; recall that optical level corrections will be provided by the WFSC system. From a materials perspective, it can be assumed that the DPTM can be constructed from either CFRP or could be 3-D printed on-orbit (when the technology is sufficiently mature). A mass of 75kg is assumed for the DPTM, based on the similarity in the design of the DPTM with that presented in Ref. [4].

Segmentation of the PM surface into identical hexagons introduces a variable gap width between segments that impacts the geometry of the backplane structure and the telescope's optical performance; thus, a key structural requirement that needs to be determined is the clearance that the truss needs so as to conform to the desired radius of curvature of the segmented PM (rule of thumb being that radius of curvature is twice the focal length). This investigation into DPTM will need to be pursued within SSC's deployable structures group in a future study on large space telescopes based on their relevant structural requirements [31]. Based on work presented in Ref. [4], a sparse tessellation for arranging the DPTMs is chosen; the justification here is that the sparse geometry includes fewer redundant truss members compared to a full tessellation. Further, Ref. [4] also informs us that the orientation of each truss module remains consistent in the sparse case whereas in the fully filled case, they must alternate which side faces upward and therefore must include two different DPTM configurations for interconnects and mirror attach points. Also in a sparse tessellation of the truss backplane structure, each truss module has a hexagonal depth that is equal to the side length of the hexagon [4]; for the mirror modules, this could be $\sim$2.5m. Lastly, [4] tells us that the interface of such a truss with its corresponding mirror module would be at the midpoint of the outer ring of mirror segments. Note that the tes-

sellation pattern chosen for the backplane assembly has no direct impact on the optical imaging capabilities of the system.

In total, the full PM backplane includes eighteen DPTMs; the trusses form two rings around a central hexagonal hub. This hub would be part of the first spacecraft launched in the assembly sequence and might include solar array attachment points that serve the PM. Of the eighteen DPTMs, the inner ring of six modules could be pre-attached permanently to the hub to aid the initial assembly process. In other words, these six DPTM would not need to be placed by the robot; they would be placed in their desired locations prior to launch and will deploy on-orbit.

2.2.3 Deployable Secondary Mirror

As discussed earlier, the end-game telescope's SM has an axial separation distance of 4.55m from the PM; this was determined from the equations for the R-C system. This leads to another key challenge: that of the deployment of this SM. One potential solution for deploying a SM was involves using stowed linkages in some of the DPTMs (which make up the PM backplane truss structure) to construct an appropriate support structure. As this is clearly a complicated assembly process that is difficult (if not impossible) to achieve with a single manipulator, it was determined that further investigation into a solution based purely on space deployable structures was necessary. Such a solution could then meet the following requirements: the SM and its connecting structure should not require robotic assembly; the overall structure should be easily stowable for launch; the deployable structure must be rigid, thermally stable, and lightweight; and space heritage on long-span deployable systems design must be exploited, if available.

Based on these requirements, a deployable mast is now presented as the adequate solution, given its demonstrated use in space at lengths exceeding the required separation distance for the end-game telescope. This approach is significantly less complex and does not require the use of a robotic manipulator. The proposed system meets all of the above identified requirements. Deployable masts are a class of articulated truss that can be stowed in a small volume and expanded into long, slender, and stable booms. Their greatest benefit is their compression ratio: masts can be packed to a fraction of their deployed length while being modestly wider than their deployed width. Current research is on masts that can be deployed with a repeatability of tip position that is no more than 1mm over 60m. At the 4.55m span necessary for the end-game telescope, it might be possible to achieve a precision of the order of tens of microns. Higher precision in the deployment is desirable for large focal length optical imaging systems, but it is believed that the SM will also require tens of nanometres level precision in tip/tilt/piston actuator technology to meet the optical performance requirements. The Nuclear Spectroscopic Telescope Array (NuSTAR) mission's 10m deployable mast, used for a X-ray telescope, is the most recent example of the use of such structures in space [32]. The proposed end-game deployable mast will be based on the system used in the SRTM for radar data collection in 2000 [33], which exhibited 1mm tip position accuracy over its 60m span. The mast is made from CFRP, stainless steel, alpha titanium, and Invar; it consists of 87 cube-shaped sections (also called bays) with a total mass of 360kg (the antenna systems are an additional 1340kg). This indicates the suitability of the structure for the application; the SM is assumed to be a 2.4m hyperbolic mirror, made of Be; based on the areal density of Be, its mass is determined to be 90.51kg. The free-end of the truss will have the SM mounted to it, prior to launch . From an operational perspective, the truss will deploy bay-by-bay out of a canister to a length of 4.55 meters. In keeping with 20:1 compression ratio of the SRTM mast, the canister itself will be $\sim$0.25m long. The canister houses the mast during launch; it also deploys and retracts if needed to protect the mast during servicing or maintenance operations. In the SRTM, a distance measurement unit on the attitude and orbit determination avionics was used to measure the length of the mast to within three millimetres by detecting a corner-cube reflector; in the case of the end-game telescope, the WFSC subsystem could also perform as a metrology instrument to assess the mast's deployment and also correct the secondary's position via the actuators.

Other options were also considered but are not at a sufficient level of technological maturity or are much riskier. For example, the deployment of the FPA of the end-game telescope could be achieved by using a deployable CFRP boom with slotted hinges, as will be demonstrated in the AAReST mission. The current limitation of this technology is that it is yet to be demonstrated to the boom lengths desired for the 25m end-game telescope. In the AAReST mission, the CRFP boom is 1.16m when fully deployed [34]. Yet another approach could be formation flying the SM as proposed in Ref. [4], where Lee et al also state that the approach is better suited for telescopes with apertures greater than 19m as opposed to using deployables as the threshold corresponding to structural deformations exceed the limits of a typical control system. However, such an analysis is dependent on several factors such as magnification of the telescope (which drives the separation distance between mirrors). Indeed, attitude control systems could be capable of the precision needed for optical requirements but given its lack of space heritage/maturity, it does not meet the fourth requirement and thus is not considered

for the end-game telescope; as European Space Agency (ESA)'s Project for On-Board Autonomy-3 (PROBA-3) mission develops, this could be revisited as an alternative to the deployable mast. Formation flying systems also add complexity, are a potential point of failure, and drive up the risk, cost, and power consumption of the mission. Ultimately, determining the suitability of the canister-mast deployable system is one that should be further analysed within SSC's deployable structures group. Separately, autonomous high-precision formation flying should also be investigated so as to develop appropriate guidance and control (G&C) algorithms as this will become necessary for separation lengths in the range of hundreds of meters. The research to address this technological need of formation-flying based alignment of the FPA and the PM can also be performed within SSC through experiments on the air-bearing table. Formation flying also has applications that are broadly relevant to EO (i.e., not just for SM positioning) and thus developing the local expertise in this area would be beneficial to all parties.

Given its established flight heritage as the most rigid structure to have flown in space, its comparably higher Technology Readiness Level (TRL) to the slotted hinge mechanism and formation flying, and its need to not be assembled by the robot, the mast-in-canister system is chosen to deploy the SM. The mass and length of each bay of the mast in its deployed configuration is determined from the details given for the SRTM; the resulting specifications of the mast and SM are shown in Table 3 below. At this point, novel actuator technology development is not likely to be needed for the positioning of the SM as the same technologies proposed for the PM segments should be sufficient for position and shape control of the SM.

Parameter	**Quantifier**	Units
Bay mass	4.1	kg
Deployed length of one bay	0.7	m
Total number of bays in mast	7	bays
Mast deployed length	9.7	m
Mast compression ratio	20:1	-
Mast mass	29	kg
Secondary mirror mass	90.5	kg

Table 3: Deployable mast and SM sizing.

2.2.4 FPA

The FPA is the portion of the telescope where the imaging electronics are located. Its location at the image plane also dictates where the wavefront sensors are situated to enable the wavefront sensing and control to precisely align the segmented mirrors to form a coherent surface and accurately capture images with the fully assembled telescope. In addition to the wavefront sensors, an array of CMOS detectors is also located at the focal plane. Each of these detectors has pixels of size 1.4μm, making them ideal for measurement of visible wavelengths. Each detector has 4096×4096 pixels (16 megapixels) and there are 625 detectors arranged in a 25-by-25 array to meet the user defined field-of-view (FoV). Each detector is assumed to have a mass of 6 grams; the FPA will also include the wavefront sensors and have a total mass of 9kg. A summary of the FPA is presented in Table 4; the assumed sensor here is the Teledyne-E2V Emerald 16M [7].

Parameter	**Quantifier**
Pixels in CMOS detector	16 megapixels
Pixel size	1.4μm
Total number of sensors	625 sensors in 25-by-25 grid
Total sensor mass	3.8kg
SiC backing plate mass	5kg
FoV	100km^2

Table 4: Focal plane assembly specifications.

2.2.5 Thermal Considerations

At GEO, the Earth's influence is almost negligible except for the shadowing during eclipses, which can vary in duration from zero at solstice to a maximum of 1.2 hours at equinox. Long eclipses influence the design of both the spacecraft's insulation and heating systems. The seasonal variations in the direction and intensity of the solar input have a great impact on the design, complicating the heat transport by the need to convey most of the dissipated heat to the radiator in shadow, and the heat-rejection systems via the increased radiator area needed.

Protection of optics and instruments is a key issue in the design of space telescopes and the classic approach of having highly absorbing baffles, such as those on the HST or the High Resolution Imaging Science Experiment (HiRISE) on NASA's Mars Reconnaissance Orbiter (MRO) [35], is assumed in this study for the SM and the FPA. However, a new category of reflective baffles developed for Bepi-Colombo, which tries to reject as much solar power as possible and absorb as little as possible, could be another viable alternative [36]. The protection of the primary mirror segments is considerably more challenging and an open problem: one approach could be to use a formation flying sunshield which should be designed to protect the PM segments but not obstruct the solar panels.

2.2.6 *Telescope System: Block Diagram and Sizing Summary*

Fig. 5 shows the system block diagram of the entire space telescope assembly. Note that the PMA comprises eighteen DPTMs (that make up the backplane) and a corresponding number of mirror modules for the PMA; these are not shown in a recurring manner in the block diagram for sake of brevity. The DPTMs are connected to the spacecraft structure via connector interfaces; similarly, connector interfaces also enable attachment of mirror modules to DPTMs. The SM is mounted to one end of the deployable mast, which is part of the spacecraft structure. The FPA is similarly structurally attached to the spacecraft; the fine guidance sensor (FGS) also has a data link between the spacecraft's attitude determination and control system (ADCS) subsystem for precision pointing.

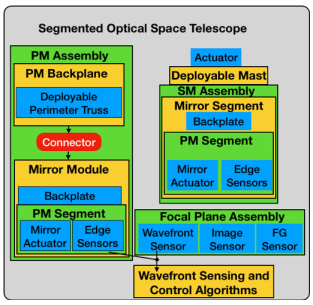

Fig. 5: System Block Diagram of Space Telescope.

A summary of the space telescope is provided in Table 5.

OTA system element	Mass (kg)	Comments
PM module	592	19 hexagonal segments with mirror actuators.
25m PMA	10662	Made of 18 modules (342 segments).
PM backplane	1350	Comprises 18 DPTMs to support PMA.
Deployable mast	29	Supports the SM
SM	90	2.4m monolithic hyperbolic SM.
FPA	9	Hosts the imaging and wavefront sensors

Table 5: Sizing summary of 25m telescope elements.

3. End-game Mission Analysis

In this section, a preliminary design and analysis for the end-game mission are presented. The mission analysis fits the following requirements:

1. the assembly shall be performed without generating debris;
2. the primary mission is to perform persistent surveillance EO from GEO with a spatial resolution of 1m which is assumed to require a primary mirror of 25 m diameter;
3. the mission shall be designed to have a nominal lifetime of ten years;
4. the system shall be designed with serviceability and modularity in mind, so that it can be serviced or 'upgraded' during and/or after the nominal mission;
5. the proposed mission shall comply with the UK Space Agency (UKSA) legal, licensing and regulatory framework in order to be eligible for a UK space licence (Note: This shall include UK Space debris mitigation standards); and
6. The estimated launch for the primary mission is 2035.

3.1 Orbit of assembly and launch vehicle

Initially, two options were considered for the orbit at which assembly is performed: at GEO (the intended operational orbit) or at LEO followed by a transfer to GEO. Firstly, there are remarkably different thermal challenges of maintaining the telescope at LEO when compared to GEO, which were discussed earlier in the section addressing mirror materials. Secondly, the necessary ΔV to get from LEO to GEO would also make this mission significantly more cost-prohibitive. Thirdly, though the entire telescope could hypothetically fit in a single launch vehicle to LEO when considering mass, launches to LEO are primarily volume constrained. Thus, the assembly phase would likely require more than a single launch to LEO. Lastly, the rendezvous and docking (Rv&D) manoeuvre necessary between a space tug and telescope system for the LEO-GEO transfer would also introduce unnecessary risk to the assembled PMA.

Assembly in GEO offers at least two important advantages: assembling the persistent EO telescope in its final operational orbit is the first of these, which eliminates the use of the tug for transferring between orbits. The second advantage is that the robotic assembly process can itself be persistently monitored/supervised thus permitting

round-the-clock monitoring of the s/c system and increasing mission safety. The disadvantage of GEO assembly is that it requires multiple launches that necessitates multiple spacecraft proximity maneuvers, which is also anticipated with LEO-based operations. On account of these reasons, assembling the telescope at GEO is the preferred option.

When accounting purely for mass delivered to GEO, either a New Glenn or Ariane 64 launch vehicle could be used for the mission; however, the trades between these vehicles was performed in Section 2 and the New Glenn was identified as the appropriate launcher. The New Glenn's fairing capacity is better suited for a cost-effective mission to GEO and is thus the chosen launch vehicle. From a payload-to-orbit perspective, the New Glenn could achieve the assembly in four launches to Geostationary Transfer Orbit (GTO) followed by a transfer to GEO; these aspects are analysed in the next subsection. By the 2035-execution date for this end-game mission, direct-to-GEO may also be an option available with New Glenn and its competitors [37]; however, this situation is not considered in this analysis.

3.2 Propellant budget to GEO

The New Glenn rocket has a payload capacity of 13 tons to GTO; then, getting to GEO requires additional propulsive manoeuvres for which a two-impulse Hohmann transfer is chosen. Thus, a portion of the launcher's capacity is dedicated to the propellant which can be easily determined. An approximate ΔV of 2km/s is assumed to determine the propellant budget required for: orbital transfer from GTO (assuming a two-impulse Hohmann transfer); and station-keeping at GEO.A hydrazine/NTO bi-propellant is assumed for the GEO transfer which results in a payload beginning-of-life mass of up to 6996kg (i.e., mass of robotic s/c delivered to GEO) and propellant mass of 6004kg.

3.3 S/C dry mass

The geometry of the spacecraft is driven by the geometry of the payload and the New Glenn's launch fairing diameter; the latter forces the width of the s/c to be $\sim$6.2 m. Of the payload elements, the PM module is the main design driver for the spacecraft's geometry; based on Fig. 3, there are two options for the s/c shape: a cube or a hexagonal prism. A hexagon is preferred for the base s/c as it permits a little larger volume compared to cube for the same quantity of material. It also offers greater flexibility for the end-over-end walker's manouevring; and lastly, the arrangement of the inner DPTMs in the backplane structure forms a hexagon gap in the middle.This also drives the central hub s/c to be hexagonal as it may facilitate easier placement of mounting interfaces for the DPTM. Note that, the volume of the DPTMs and manipulator in their stowed configurations are negligible in comparison to that of the mirror modules. In other words, their stowage is believed to not impact as heavily as the mirror modules on the launch configuration and spacecraft's geometry; this is due to the fact that the robot and DPTMs can be folded into more compact configurations when not in use.

The dry mass of the spacecraft is driven by two factors: the payload-to-bus dry mass ratio for every launch; and the beginning-of-life mass at GEO. The beginning-of-life mass is already known from the sizing of the propellant budget. However, the following assumption is made regarding bus dry mass and payload elements: at beginning-of-life, the s/c bus mass-to-payload ratio shall not exceed unity. This is based on the space mission design methodologies discussed in Refs. [13] and [38]. It is also in keeping with the SSTL-42 brochure [39], which indicates a bus dry-to-payload mass ratio of 1 is feasible. This assumption and the selected launch vehicle's delivery capabilities can be formalized in the following set of equations, respectively:

$$m_{S/C} + m_{PL} = m_{b.o.l} \quad [8]$$

$$\frac{m_{S/C}}{m_{PL}} \leq 1, \quad [9]$$

where $m_{S/C}$ is the dry mass of the spacecraft bus, m_{PL} is the payload mass, and $m_{b.o.l}$ is the beginning of life mass of the system at GEO. Substituting for m_{PL} from Equation 9 into Equation 8 to solve for $m_{S/C}$ informs us that the spacecraft must weigh at least half of $m_{b.o.l}$; Refs. [13] and [38] state that the payload could be as much as 55% of the beginning of life mass. Thus, the assumed mass budget is as shown in Table 6, which gives a s/c mass of $\sim$3960kg. The spacecraft subsystem masses are also estimated based on discussions presented in Refs. [13] and [38]. Note that as a margin has not been assumed in these calculations, the numbers presented in the analysis should be assumed to be indicative for the end-game mission.

With this information regarding the masses, a mission manifest is developed for the end-game mission; this is shown in Table 7. Note that the percentage of payload mass at GEO for launch 1 is 42% whereas it is 51.4% for launches 2, 3, and 4; this is in alignment with the mass budget proposed above in Table 6. Also, though launch 1 could also accommodate 2 further mirror modules, four launches will still be necessary to assemble the PM. Thus, to maintain homogeneity in the spacecraft design and mission's ConOps, six mirror modules are delivered in each of the final three launches.

Mission element	$\%m_{b.o.l}$
Payload	52
S/C dry mass (subsystem dry masses below):	48
propulsion	6
ADCS	8
communications	4
C&DH	1
thermal	3
EPS	11
structural	15

Table 6: Assumed S/C subsystem mass budgets as % of beginning-of-life mass at GEO; adapted from statistical mission information discussed in [13] and [38].

Launch 1	
GTO to GEO propellant mass	6004kg
Base S/C	3358kg
Payload (18 DPTMs, Robot, SM, FPA)	2423kg
Total	11785kg
Launches 2, 3, and 4	
GTO to GEO propellant mass	6004kg
Base S/C	3358kg
Payload (6 mirror modules per launch)	3554kg
Total	12916kg

Table 7: End-game mission manifest

3.4 Concept of Operations

Based on the four-launch mission profile described above, the assembly sequence at GEO will be as follows. The first launch will bring the telescope system's main s/c bus, the RASTA assembly system, the deployable SM, FPA, and all eighteen of the modular backplane-forming DPTMs to GEO. The selected robotic assembly agent is an end-over-end walking robotic arm, which was based on considerations and trade-offs between several different architectures. The robot attaches each stowed truss, to the base s/c (for the inner ring) or to other trusses (for the outer ring), by exploiting this end-over-end walking ability to relocate itself and extract the truss from the base s/c. The physical connections between the trusses, robot, and base s/c are facilitated via the standardized electromechanical connector interfaces. After each truss is placed in its desired location, it auto-deploys to its unstowed configuration. Alternatively, the robot can also be utilized to unfurl the truss once it is attached to the hub. The key difference between this robotic assembly approach and the one discussed in [4] is that the truss is only deployed after it is attached to the hub in the proposed end-game mission, which creates the potential of deploying without dual-manipulators. Dual-handedness drives up the mass and cost of the robotic architecture and the mission. It also introduces unnecessary control complexity that is only now being developed for space applications through the Robotic Refueling Mission (RRM) [40]. Thus, to maintain a low degree of complexity in the robot tasks and operations, the auto-deployment approach for trusses is preferred over manipulator-based deployment.

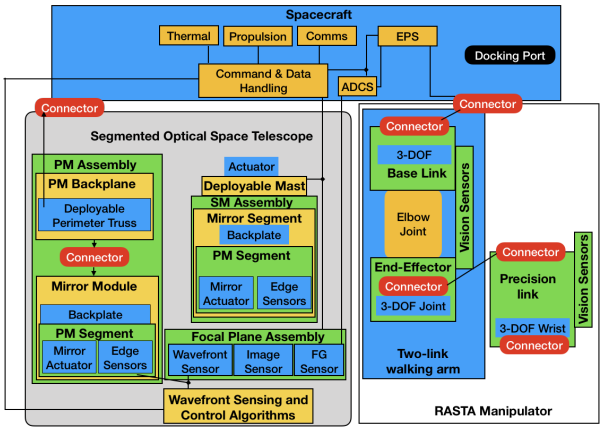

Fig. 6: End-game mission: systems block diagram.

Following the assembly of the backplane, a second s/c (called StorageSat, which is short for Storage Satellite) will Rv&D with the hub spacecraft; this StorageSat will deliver 6 mirror modules that the robot then places on the deployed trusses and, in total, three launches will be needed. Assessing the requirements for this Rv&D system is currently out of the scope of this study but could be pursued in the future; such work would build on the foundational work performed by SSTL and SSC in [41] via the National Space Technology Programme (NSTP) study. The third and fourth launches will have an identical profile to launch number 2; each launch would deliver six additional mirror modules for the robot to complete the assembly process. Then the SM is deployed and the commissioning phase of the telescope will be initiated. The systems block diagram of the robotically assembled telescope is shown in Fig. 6 and full ConOps of this assembly architecture is shown in Fig. 7.

The end-game mission architecture has been developed but there is a considerable gap in operating this telescope that needs further consideration: the design of a sunshield that will allow the maintenance of the optical structure at a

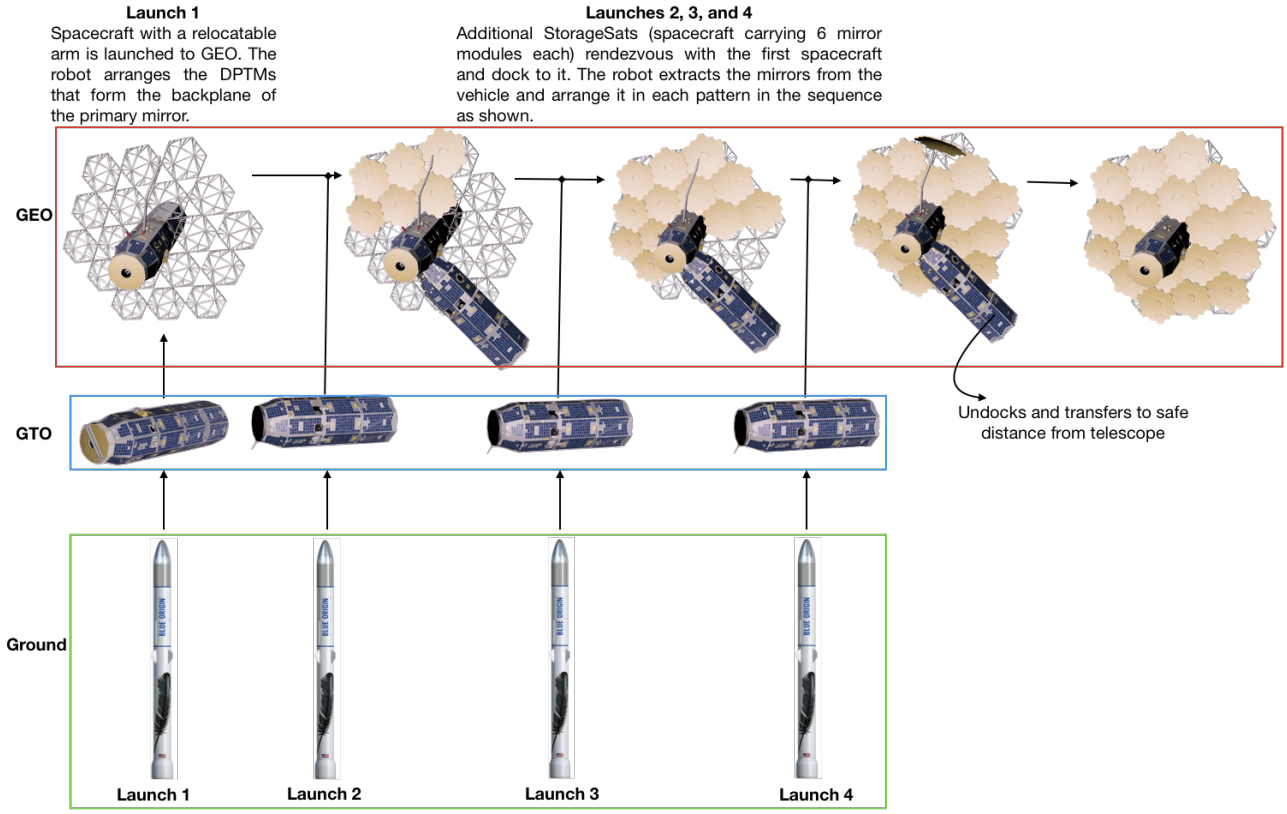

Fig. 7: ConOps of the assembly of the PM of the telescope.

constant (or near-constant) temperature. This will need to be developed. Several potential solutions have been discussed and this conversation will continue to develop as, like many other aspects of robotic OOA, the problem is an unprecedented one. The only other detailed OOA study [4] has proposed the use of a formation flying sun-shield. This approach is reasonable for a telescope at the Sun-Earth Lagrange points as both celestial bodies are always on the same side of the spacecraft. However, the Sun's position relative to the telescope changes more drastically for a telescope at GEO. Thus, a set of deployable sun-shields attached to the main spacecraft might be needed for a telescope in GEO or a set of formation flying sun-shields in close proximity of the spacecraft may be necessary. This work clearly needs further attention and it is a conversation that might continue to receive attention in the coming future.

4. Roadmap of Demonstration Missions

A set of three missions are proposed here, which present a phased build-up of capabilities towards the end-game mission.

4.1 Mission 1: Testing of Space Robot in LEO

4.1.1 Mission requirements

The primary objective here is the on-orbit qualification of a robotic system and standardized grappling/connector interface; specifically, this mission will test the robot arm's ability to use its sensor systems (cameras and light detection and ranging (LiDAR)) to identify a co-operative target (i.e., the standardized interface) and then autonomously plan/execute a manoeuvre to grapple the connector. In many ways, this experiment is similar to the Manipulator Flight Demonstration experiment performed by Japanese Aerospace Exploration Agency (JAXA), where an Orbital Replacement Unit (ORU) was manipulated [42]. The user requirements for the proposed mission are as follows:

1. The mission shall be a robotic arm and connector demonstrator in LEO to enable a future OOA-based EO mission.
2. The s/c shall be compatible with a low-cost launcher (as either a primary or secondary payload).
3. The total mass of the launched system must be under 150kg so as to meet secondary payload requirements.

4. The mission shall launch by 2022.
5. The orbit shall be circular with an altitude lower than 400 km (i.e., lower than the altitude of the ISS).
6. The proposed mission will comply with the UKSA legal, licensing, and regulatory frameworks in order to be eligible for a United Kingdom (UK) space licence (Note: This shall include UK space debris mitigation standards).

The associated ConOps for this mission is described in Fig. 8, which shows a set of four connectors on the base of the s/c for the robot to relocate itself; however, for a simpler demonstration, it is envisioned that two connectors will be sufficient and the robot can demonstrate attaching, detaching, and re-attaching between two connectors. Demonstrating end-over-end walking with additional interfaces would be a minor-extension to the mission operations and one that would significantly advance the capabilities of the robotic system for subsequent demonstration and end-game missions.

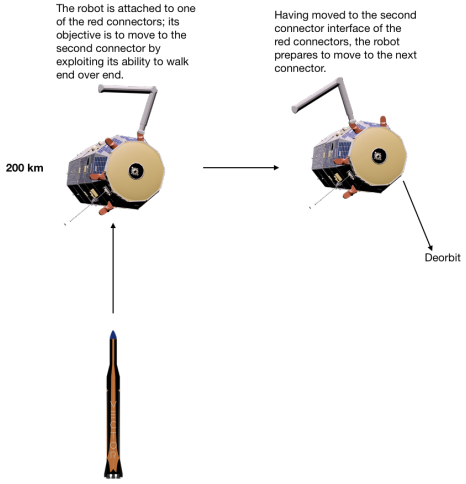

Fig. 8: ConOps of Mission 1, demonstrating the end-over-end walking robot system.

4.1.2 Sizing

An appropriate platform for such a test would be the system designed in Ref. [43] within SSC; the system comprises a 12U SmallSat of 19.7kg with a small robotic arm (∼3.3kg) mounted upon it; as an alternative, the fig/Demonstration of Technology-4 (DoT-4) [44] platform of 35kg could be another candidate for the s/c bus. The robotic arm in Ref. [43] has a full span of 0.5m and a mass of under 23kg (without sensors). An external vision system will enhance the situational awareness for safe manipulation by and relocation of the robot. In addition, a sensor suite will also be required on its end-effector for relative navigation of the arm to the cooperative target object. The addition of these sensor packages and a connector interface for testing will increase the mass of the system for this first mission. Currently, the use of a hybrid optical sensing system, such as that used in a recent SSTL-led Rv&D study [41], is assumed to be appropriate for the external sensor package in this demonstration mission. Two such packages on the perimeter of the s/c, each weighing 4kg [41], and a connector could be achieved in under 13kg. In addition to the connector and external sensor package, a vision system on the end-effector of the robot to assist with the visual servoing to the cooperative target. A potential candidate for such a sensor could be the Intel RealSense RGB-D sensor [45], which weighs under 10g but is yet to be space qualified. The total payload mass (sensors, connector, and 3.3kg robot arm) would be 16.4kg. Thus, assuming a bus mass of 19.7kg (as per [43]) gives a reasonable mass ratio of payload to s/c of 0.83 for this mission and a total mass of 36kg.

The Vector-R launch vehicle appears to be an ideal choice for this mission; it is capable of placing up to 60kg in LEO at an estimated launch cost of $1.5 million. However, there are also other launch options for this mission. The envelope of the 12U satellite (0.3m $\times$ 0.2m $\times$ 0.2 m) along with the robot arm would be well within the permissible envelope of an Evolved Expendable Launch Vehicle (EELV) Secondary Payload Adapter (ESPA) system [46]. It might however be more amenable to the miniSHERPA system, which is for s/c under 50kg and a volume of 0.4m $\times$ 0.4m $\times$ 0.6m [47]; the mini-SHERPA is a space tug with a commercial derivative of the ESPA Grande ring for deploying small payloads. A Polar Satellite Launch Vehicle (PSLV) piggyback may also be considered for this mission though information on the permissible payload volumes was not provided online for this launch vehicle. As costs were not readily available for any of these launch options, the Vector-R is the assumed launch vehicle (as shown in Fig. 8). The block diagram for this system is the same as that shown in Fig. 6 but without the telescope system and thus is not repeated for sake of brevity.

4.2 Mission 2: 2m telescope at LEO

4.2.1 Mission Requirements

The primary objective of mission 2 is to demonstrate the robotic OOA of a HST-class imager in LEO. The mission requirements are:

1. Perform the assembly of a keyhole-class telescope without generating debris.
2. All manipulable objects are assumed to be cooperative, i.e. they communicate their pose to the robotic

system so as to facilitate their manipulation.

3. Develop an architecture that aligns with the architecture needed for the end-game while also building on the capabilities of the first mission demonstrating the robot and connector interface.

4. The mission shall be compatible with a low-cost launcher.

5. The proposed mission shall comply with the UKSA legal, licensing, and regulatory framework in order to be eligible for a UK space licence (Note: This shall include UK space debris mitigation standards).

6. The estimated launch for the primary mission is 2025.

7. The mission will be situated in LEO, at an altitude of 400km.

4.2.2 Telescope design

For the purpose of this study, spatial resolutions of 0.05m from 200km or 0.15m from 500km Sun Synchronous Orbit (SSO) qualify a telescope to be of 'keyhole' class. Assuming an identical detector to that used in the end-game missions and the aforementioned resolutions, the focal length for a keyhole telescope at either altitude is $\sim$11.2m and 9.3 m, respectively; the corresponding aperture sizes for the primary mirror are 2.68m and 2.24 m, respectively. Indeed, the aperture size for these telescopes are in the vicinity of the Kennen-KH 11 reconnaisance satellite (upon which the Hubble design is based). To normalize the comparison between the telescopes being constructed, the mean of these apertures is chosen for the LEO telescope's PM (i.e., 2.4m) to perform the necessary trade-off between an approach with pure pick-and-place and one that involves Rv&D (i.e., an approach with at least two free-flyers to achieve telescope assembly). Given the considerably large focal lengths, once again a folded-optics R-C design is adopted for the telescope. In the subsequent design of the R-C system (based on equations presented in Section 2), a magnification factor of 10 is assumed in determining the telescope's physical attributes. Also, the SM is assumed to be hexagonal with 0.4m flat-to-flat. The deployable mast for such a telescope will comprise two bays, with a total mass of 8.28kg. The FPA is assumed to comprise 16 CMOS sensors arranged in a 4-by-4 grid giving a FoV of 0.28 degrees (2.45 km^2) and a total mass (including SiC backing plate) of 0.23kg.

The PMA is assumed to be made from 0.8m segments (6 in total); the assumed areal density of the mirror is 60kg/m^2, resulting in a 33.26kg mirror segment. A higher areal density is used here, when compared to the end-game mission, to accommodate for the perceived lack of commercial availability of JWST-class lightweight mirrors by 2025. The total mass of the PMA, including an allotment of 80% of the mirror mass for the actuators and backing plate per segment, is 359.19kg. Each mirror module with actuator in the PMA is assumed to be about 0.45m in wide and 0.8m long. Here, the standardized connector interfaces must be integrated into the design and there shall be at least two such interfaces per module: one to to facilitate manipulation by the robot arm and the other to connect the module to the DPTM. The backplane is made of 6 such DPTMs, at a total mass of 42kg.

4.2.3 Robotic system

The robot arm in this case shall be identical in design to that proposed for the end-game mission: a two-link end-over-end walker and a smaller one for dexterous tasks that attaches to the larger span two-link walker. Each links on the larger robot will be 0.45m and made of polyether ether ketone (PEEK). The link for the small arm will be 0.2m, giving the robotic system a full span of 1.1m when all three links are connected. This is presumed to be sufficient to manipulate the 0.8m segments but will need to be clarified in a future study. The mass of the robot's links and sensors is estimated to be 25.5kg. Note that, at these smaller scales, it may suffice to have only the two-link arm for dexterous manipulations. However, in developing the concept towards a system for larger assembly as in the end-game, it is recommended to maintain homogeneity in the robotic system design.

4.2.4 Launch vehicle selection and mission sizing

The specifications of this LEO imager are summarized in Table 8 below. The total payload mass of 449kg (including the robot), the assumed mass ratio between the payload and s/c, and the desired launch vehicle determine the s/c sizing/design in this case. The s/c mass is derived based on the budgets presented in Table 9.

Based on a survey of launch vehicles [48], the Firefly Alpha [49] is identified as the most appropriate launcher for this s/c given its ability to place systems at either 200km or 500km LEO. Though the PSLV is another option, pricing indicates that two launches of the Firefly Alpha can be secured for less than one PSLV launch [48]. The Firefly's fairingcan only fit a fully assembled telescope of under $\sim$2m. Thus a 2.4m telescope will need to be assembled on-orbit but can be packaged in its fairing. It was also determined that the fairing capacity will be sufficient to permit a s/c that stores mirrors within it (along with the more negligible volumes of the DPTM, robot, and deployable SM). The capability to store mirrors offers protection during launch and separation, thus

making it more preferable than a deployment-based approach. Note that, as the Firefly has the capacity to lift 1000kg to 200km or 630kg to 500km, two mission scenarios are possible. In the first scenario, a single launch could bring all telescope components and robot to 200km for assembly; alternatively, a two-launch approach can be used to assemble a telescope at LEO, which would also require Rv&D of two s/c.

Parameter	**Characteristics**
Desired spatial resolution	0.05m at 200 km
Focal length	10m
PM aperture	2.4m
SM aperture	0.4m
Primary-secondary separation distance	1.67m
FPA distance behind PM	0.83m
Number of segments in primary	6
Areal density of mirror material	60kg/m^2
Total mass of primary mirror	199.54kg
Fill factor	0.82
Robotic agent mass	31kg

Table 8: 2.4m LEO telescope summary.

Mission element	$\%m_{b.o.l}$**(kg)**
Payload	53
S/C dry mass (subsystem dry masses below):	47
propulsion	1
ADCS	8
communications	4
C&DH	1
thermal	3
EPS	15
structural	15

Table 9: Assumed S/C subsystem mass budgets as % beginning-of-life mass at LEO.

Manifests for both mission options are shown in Tables 10 and 11, respectively. In regards to choosing an appropriate architecture, the single launch approach is chosen as it is both cheaper and also enables higher resolution imaging. Further, as a first mission to demonstrate assembly, it is also comparatively simpler than one requiring Rv&D.

Note that in the LEO mission context, the mass budget inherently accounts for the propellant as it is only used for station-keeping manouevres and thus would not be a significantly high proportion of the overall mission mass. Thus, the propellant for station-keeping is assumed to be any remaining capacity of the launcher. Based on this, the propellant mass fraction for option 1 is 8.1%. Similarly for option 2, the propellant mass fraction for launches 1 and 2 are upto 13.57% and 21.16%, respectively.

LEO telescope at 200 km	
Base S/C	470kg
Payload (6 DPTMs, Robot, SM, FPA)	449kg
Total	919kg

Table 10: LEO mission manifest option 1: Single launch to 200 km

Launch 1	
Base S/C	296kg
Payload (3 DPTMs, 3 PMs, Robot, SM, FPA)	248kg
Total	544kg
Launch 2	
Base S/C	296kg
Payload (3 DPTMs, 3 PMs)	201kg
Total	497kg

Table 11: LEO mission manifest option 2: Two launches to 500 km

4.2.5 ConOps

Fig. 9 shows the ConOps of the assembly of the PM.

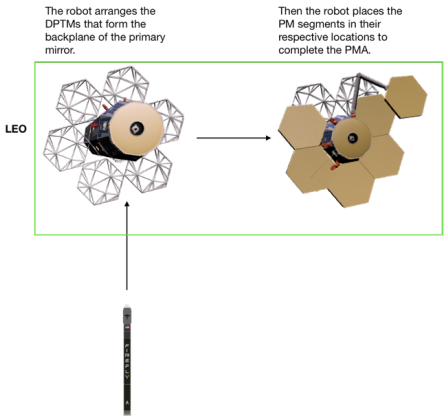

Fig. 9: ConOps LEO 2.4m telescope assembly.

The assembly sequence of this single launch mission is similar to the end-game mission. The robot first assembles the 6 DPTMs along the base spacecraft using its ability to relocate; following truss deployment, the robot proceeds to place the mirrors in the appropriate locations. Upon completion of the assembly, the secondary mirror is deployed and the commissioning phase for telescope operations begin. The block diagram for this mission is identical to that shown in Fig. 6.

4.3 Mission 3: 5m telescope in GEO

4.3.1 Mission Requirements

The proposed GEO OOA demonstration mission has the following set of requirements:

1. The primary mission objective is to demonstrate robotic systems technologies by constructing a 5m Earth Observation telescope from GEO.
2. The assembled telescope shall be a scaled version of the end-game telescope.
3. The robotic agent used shall be a scaled version of the end-game's assembly agent.
4. All manipulable objects are assumed to be co-operative, i.e. they communicate their pose to the robotic system to facilitate their manipulation.
5. The proposed mission will comply with the UKSA legal, licensing, and regulatory framework in order to be eligible for a UK space licence (Note: This shall include UK Space debris mitigation standards).
6. The mission shall have a lifespan of ten years.
7. The estimated launch for this demonstration mission is 2030.

4.3.2 Telescope design

There are no specific user requirements for imaging with this mission as its primary objective is the assessment of challenges with assembling a larger telescope in the GEO environment. As this mission shall be designed to align as closely as possible to the end-game mission, a R-C telescope design is chosen. Such a 5m optical EO telescope at GEO (36,000km) will have a resolution of 5m if operating in the optical wavelength, which would be better than the current highest resolution GEO-based imager currently on-orbit, the Gaofen-4; it has a 50m resolution in visible wavelength [50].

For the proposed imager, the primary-secondary separation distance is 2.01m (this can be derived from the Cassegrain design equations in Section 2 by assuming a magnification of 10). Fig. 4, sans the centre-most mirror segment, shows the schematic of the PM for this 5m telescope, which comprises 6 mirror modules. In each module, each mirror is assumed to be of 1m flat-to-flat length. It is evident from Fig. 4 that there are two fundamental module types (each module comprises 3 mirrors) that make up this 5m telescope:

1. Two modules, shown in blue and green in Fig. 4, represent one of the modular configurations; this is referred to as type-1 module, and
2. the four sets shown in magenta and cyan make up the other type of modular arrangement and are referred to as type-2 module; the yellow module in Fig. 4 can similarly comprise two type-2 modules.

All mirror segments are assumed to be 1m in flat-to-flat length and have a mass of 30.31kg (here, an areal density of 35kg/m^2 is assumed). Each mirror (and, therefore module) has an assumed thickness of 0.45m.

The mission is designed to replicate many aspects of the end-game assembly mission (whilst using a smaller aperture design) namely: robotically assembling groups of mirrors (as opposed to placing a single hexagonal mirror segment in every move as done in the LEO OOA mission); and constructing a telescope with more than one-level/layer of tessellation in the PMA. Just as in the end-game telescope, the mirror modules will be connected to the base-spacecraft via DPTMs that have been placed by the robot along the s/c. The standardized connector interface will be used to establish physical connections between the modules to the spacecraft and/or the arm. In total, six pick-and-place operations will be performed by the robotic arm to assemble the primary mirror (in addition to six similar motions to assemble the backplane using DPTMs). When an assembly task is out of the robot's current working volume, the robot shall relocate itself so as to resume with the assembly objective.

As with the end-game telescope design, a deployable mast system is used to deploy the SM after the PM is assembled. The FPA of this 5m telescope is also designed to offer a FoV of 100km^2; for this, the same CMOS sensors used in the end-game telescope are selected, arranged in a 5-by-5 grid (i.e. 25 sensors in total). Note that the spatial resolution achievable with such a 5m visible wavelength telescope operating at GEO is 5m. A table summarizing the sizing of the various elements of this telescope are shown below in Table 12. The mass of the DPTM here is assumed to scale linearly as a function of the deployed length of the DPTM used in the end-game telescope; this approximation is made because the specifications of an exact model of the DPTM is unavailable at this time and requires further research.

OTA system element	Mass (kg)	Comments
PM module	94	3 hexagonal segments (1m flat-to-flat) with mirror actuators.
5m PMA	312	Made of 6 PM modules; 18 mirror segments in total.
PM backplane	270	Comprises 18 DPTMs, each of 15kg; supports the PMA.
Deployable mast	12	Supports the secondary mirror
SM	4	0.5m monolithic hyperbolic secondary mirror.
FPA	0.36	Hosts the imaging and wavefront error sensors

Table 12: Sizing summary of 5m telescope elements.

4.3.3 Robotic system

The robot shall be identical in design to that proposed for the end-game mission: a two-link end-over-end walker and an extensible smaller arm for dexterous tasks. The links on the walker will be 1m each and made of PEEK. The link(s) for the dexterous arm will be 0.5m. The mass of the robot arm's booms and sensors (assumed to be 20% of the total mass of the links) is estimated to be 53kg.

4.3.4 Propulsion and launch vehicle selection

Three low-cost launch vehicles with the ability to deliver payloads to GEO were identified, namely: Geosynchronous Satellite Launch Vehicle Mark III (GSLV-III), Ariane 62, and Falcon-9. As these vehicles only deliver to GTO, a trade between several different launchers was performed based on mass-to-GTO. As with the end-game telescope, the bipropellant hydrazine/NTO system was selected for the Hohmann transfer to GEO. Similarly, the sizing budget from Table 6 is assumed for all launchers and a ΔV of 2 km/s was assumed; this budget also similarly accommodates for the GTO-to-GEO transfer and ten-year station-keeping propellant mass estimation in the associated calculations.

It was found that the GSLV-III's beginning-of-life mass is insufficient to achieve the mission in one-launch; using a multi-launch approach would drive up the cost of the mission and thus it not preferred for this mission. Though the Falcon-9 allows a generous beginning-of-life mass and a comparable fairing diameter to the Ariane 62, its fairing volume is smaller than that of the Ariane 62. It may not be necessary to have the additional volume offered by the Ariane 62 but it provides a useful "cushion". Also, the decision to choose one launch vehicle over another will be based on the launcher's history of success, cost to transfer spacecraft to launch sites, any other related costs, and potential licensing tasks. Thus, the Ariane 62 is the chosen vehicle in developing the mission manifest shown in Table 13.

Ariane 62 Launcher	
GTO to GEO propellant mass	2309kg
Base S/C	1291kg
Payload (18 DPTMs and PMs, Robot, SM, FPA)	740kg
Total	4340kg

Table 13: GEO 5m demo mission manifest

4.3.5 ConOps

The assembly sequence for this demonstration mission at GEO will be similar to the single launch LEO OOA mission; the only difference here is that there are 12 additional DPTMs and mirrors that form the outer ring. The launch will bring the s/c bus, the robotic assembly agent, and modular telescope elements to GEO. Here, the robot unpacks and assembles all the DPTMs around the base s/c in a total of 18 motions. The layout of the DPTMs is identical to that of the end-game telescope, the only difference being that the demo mission DPTMs are $\sim$1m when fully deployed whereas each end-game DPTM is 5m when deployed. After truss auto-deployment, the robot places the mirror modules, beginning from the inner segments and working its way outward.

5. Conclusions

The objectives of this paper were to define four future OOA missions (including three precursors technology demonstration missions) by specifying:

1. mission and system requirements for the end-game mission of robotic on-orbit assembly of a 25 m space telescope,
2. mission/assembly architecture trades, preliminary mission analysis (sizing), baseline selection
3. technology/subsystem definitions (block-diagram level), and
4. form the concept of operations.

To this end, the paper began by evaluating optical telescope designs from which the Ritchey-Chretien telescope

was found to be an ideal design to meet the user requirement of 1 m spatial resolution from GEO for the end-game telescope. Challenges associated with imaging in the optical wavelengths for this system were assessed, technologies needing development were identified, and a trade-offs driven mission profile for robotic on-orbit assembly were presented. Then a full mission architecture for its OOA was also presented. This paper then proposes and analyses a set of three demonstration missions, which serve to pave the way for the technology demonstrations necessary for achieving the end-game telescope assembly. The plan of the authors is to focus on the first mission addressing the in-orbit demonstration of a relocatable space robot.

Acronyms

ADCS: attitude determination and control system
AAReST: Autonomous Assembly of a Reconfigurable Space Telescope
Be: Beryllium
C&DH: command and data handling
CalTech: California Institute of Technology
CFRP: carbon fibre reinforced plastic
CMOS: complementary metal-oxide-semiconductor
ConOps: Concept of Operations
CTE: coefficient of thermal expansion
DoF: degrees-of-freedom
DoT-4: fig/Demonstration of Technology-4
DPTM: deployable perimeter truss modules
EELV: Evolved Expendable Launch Vehicle
EO: Earth observation
eps: EPS electrical power subsystem
ESA: European Space Agency
ESPA: EELV Secondary Payload Adapter
FoV: field-of-view
FPA: Focal Plane Assembly
G&C: guidance and control
GEO: Geostationary Earth Orbit
GSLV-III: Geosynchronous Satellite Launch Vehicle Mark III
GTO: Geostationary Transfer Orbit
HST: Hubble Space Telescope
i-Boss: intelligent Building blocks for on-orbit satellite servicing and assembly
IR: infrared
ISS: International Space Station
JAXA: Japanese Aerospace Exploration Agency
JWST: James Webb Space Telescope
LEO: Low Earth Orbit
MSS: Mobile Servicing System
NASA: National Aeronautics and Space Administration
NuSTAR: Nuclear Spectroscopic Telescope Array
OOA: on-orbit assembly
ORU: Orbital Replacement Unit
OTA: Optical Telescope Assembly
PEEK: polyether ether ketone
PM: Primary mirror
PMA: primary mirror assembly
PROBA-3: Project for On-Board Autonomy-3
PSF: point spread function
PSLV: Polar Satellite Launch Vehicle
RAMST: Robotically Assembled Modular Space Telescope
RASTA: Robotic Agent for Space Telescope Assembly
R-C: Ritchey-Chrétien
RMS: root mean square
RRM: Robotic Refueling Mission
Rv&D: rendezvous and docking
SC: spacecraft
SiC: silicon carbide
SLS: Space Launch System
SM: secondary mirror
SMAP: Soil Moisture Active Passive
SPDM: Special Purpose Dexterous Manipulator
SRTM: Shuttle Radar Topography Mission
SSC: Surrey Space Centre
SSO: Sun Synchronous Orbit
SSRMS: Space Station Remote Manipulator System
SSTL: Surrey Satellite Technology Limited
TRL: Technology Readiness Level
UKSA: UK Space Agency
ULE: Ultra-Low Expansion® glass
WFSC: wavefront sensing and control
LiDAR: light detection and ranging

References

[1] ([Accessed: 28-02-2019]) HST: ESA factsheet. [Online]. Available: https://spacetelescope.org/about/general/fact_sheet/

[2] ([Accessed: 28-02-2019]) JWST: NASA website. [Online]. Available: https://jwst.nasa.gov/about.html

[3] ([Accessed: 28-02-2019]) MSS: NASA website. [Online]. Available: https://www.nasa.gov/mission_pages/station/structure/elements/mobile-servicing-system.html

[4] N. N. Lee, J. W. Burdick, P. Backes, S. Pellegrino, K. Hogstrom, C. Fuller, B. Kennedy, J. Kim, R. Mukherjee, C. Seubert *et al.*, "Architecture for in-space robotic assembly of a modular space telescope," *Journal of Astronomical Telescopes, Instruments, and Systems*, vol. 2, no. 4, p. 041207, 2016.

[5] A. Nanjangud, P. C. Blacker, A. Young, C. M. Saaj, C. I. Underwood, S. Eckersley, M. Sweeting, and P. Bianco, "Robotic architectures for the on-orbit assembly of large space telescopes," in *Proceedings of the Advanced Space Technologies in Robotics and Automation (ASTRA 2019) symposium*. European Space Agency (ESA), 2019.

[6] C. Saunders, D. Lobb, M. Sweeting, and Y. Gao, "Building large telescopes in orbit using small satellites," *Acta Astronautica*, vol. 141, pp. 183–195, 2017.

[7] ([Accessed: 28-02-2019]) Teledyne-E2V Emerald 16M. [Online]. Available: https://www.teledyne-e2v.com/content/uploads/2019/01/36956_Teledyne-E2V-CMOS-sensor-guide-update_Jan-19_v2_AW_SPREADS_WEB.pdf

[8] D. Baiocchi and H. P. Stahl, "Enabling future space telescopes: mirror technology review and development roadmap," *astro2010: The Astronomy and Astrophysics Decadal Survey, Technology Development Paper*, no. 23, 2009.

[9] ([Accessed: 28-02-2019]) Lockwood Optics: Ritchey-Chretien Cassegrain Telescope design equations. [Online]. Available: http://www.loptics.com/ATM/mirror_making/cass_info/cass_info.html

[10] J. Nelson, "Segmented mirror telescopes," in *Optics in Astrophysics*. Springer, 2006, pp. 61–72.

[11] ([Accessed: 28-02-2019]) Gemini observatory: mirror coatings. [Online]. Available: http://www.gemini.edu/node/103

[12] D. Baiocchi, *Design and control of lightweight, active space mirrors*, 2004.

[13] V. L. Pisacane, *Fundamentals of space systems*. Johns Hopkins University/Appli, 2005.

[14] L. D. Feinberg, M. Clampin, R. Keski-Kuha, C. Atkinson, S. Texter, M. Bergeland, and B. B. Gallagher, "James webb space telescope optical telescope element mirror development history and results," in *Space Telescopes and Instrumentation 2012: Optical, Infrared, and Millimeter Wave*, vol. 8442. International Society for Optics and Photonics, 2012, p. 84422B.

[15] U. Papenburg, W. Pfrang, G. Kutter, C. E. Mueller, B. P. Kunkel, M. Deyerler, and S. Bauereisen, "Optical and optomechanical ultralightweight c/sic components," in *Optical Manufacturing and Testing III*, vol. 3782. International Society for Optics and Photonics, 1999, pp. 141–157.

[16] R. Eng, J. R. Carpenter, C. A. Foss, J. B. Hadaway, H. J. Haight, W. D. Hogue, D. Kane, J. R. Kegley, H. P. Stahl, and E. R. Wright, "Cryogenic performance of a lightweight silicon carbide mirror," in *Optical Materials and Structures Technologies II*, vol. 5868. International Society for Optics and Photonics, 2005, p. 58680Q.

[17] H. Kaneda, T. Onaka, T. Nakagawa, K. Enya, H. Murakami, R. Yamashiro, T. Ezaki, Y. Numao, and Y. Sugiyama, "Cryogenic optical performance of the astro-f sic telescope," *Applied optics*, vol. 44, no. 32, pp. 6823–6832, 2005.

[18] J. W. Baer and W. P. Lotz, "Figure testing of 300-mm zerodur mirrors at cryogenic temperatures," in *Cryogenic Optical Systems and Instruments IX*, vol. 4822. International Society for Optics and Photonics, 2002, pp. 35–41.

[19] P. Bely, *The design and construction of large optical telescopes*. Springer, 2003.

[20] I. Surdej, "Co-phasing segmented mirrors: theory, laboratory experiments and measurements on sky," Ph.D. dissertation, TU-Munich, 2011.

[21] J. A. Gersh-Range, E. M. Elliott, M. D. Perrin, and R. P. van der Marel, "Minimizing the wavefront error degradation for primary mirror segments with failed hexapod actuators," *Optical Engineering*, vol. 51, no. 1, p. 011005, 2012.

[22] P. A. Lightsey, C. B. Atkinson, M. C. Clampin, and L. D. Feinberg, "James webb space telescope: large deployable cryogenic telescope in space," *Optical Engineering*, vol. 51, no. 1, p. 011003, 2012.

[23] ([Accessed: 28-02-2019]) PI-USA piezo- and voice-coil actuators. [Online]. Available: https://tinyurl.com/yy9bpyrb

[24] H. P. Stahl, "Survey of cost models for space telescopes," *Optical Engineering*, vol. 49, no. 5, p. 053005, 2010.

[25] H. P. Stahl, T. Henrichs, A. Luedtke, and M. West, "Update on multivariable parametric cost models for ground and space telescopes," in *Space Telescopes and Instrumentation 2012: Optical, Infrared, and Millimeter Wave*, vol. 8442. International Society for Optics and Photonics, 2012, p. 844224.

[26] H. P. Stahl and T. Henrichs, "Multivariable parametric cost model for space and ground telescopes," in *Modeling, Systems Engineering, and Project Management for Astronomy VI*, vol. 9911. International Society for Optics and Photonics, 2016, p. 99110L.

[27] L. D. Feinberg, J. G. Budinoff, H. A. MacEwen, G. W. Matthews, and M. Postman, "Modular assembled space telescope," *Optical Engineering*, vol. 52, no. 9, p. 091802, 2013.

[28] J. M. Hedgepeth, "Pactruss support structure for precision segmented reflectors," 1989.

[29] W. Doggett, "Robotic assembly of truss structures for space systems and future research plans," in *Proceedings, IEEE Aerospace Conference*, vol. 7. IEEE, 2002, pp. 7–7.

[30] M. W. Thomson, "The astromesh deployable reflector," in *IEEE Antennas and Propagation Society International Symposium. 1999 Digest. Held in conjunction with: USNC/URSI National Radio Science Meeting (Cat. No. 99CH37010)*, vol. 3. IEEE, 1999, pp. 1516–1519.

[31] M. S. Lake, L. D. Peterson, and M. B. Levine, "Rationale for defining structural requirements for large space telescopes," *Journal of Spacecraft and Rockets*, vol. 39, no. 5, pp. 674–681, 2002.

[32] ([Accessed: 28-02-2019]) Nustar mast. [Online]. Available: https://www.nustar.caltech.edu/page/paper_model

[33] T. G. Farr, P. A. Rosen, E. Caro, R. Crippen, R. Duren, S. Hensley, M. Kobrick, M. Paller, E. Rodriguez, L. Roth *et al.*, "The shuttle radar topography mission," *Reviews of geophysics*, vol. 45, no. 2, 2007.

[34] C. Underwood, S. Pellegrino, H. Priyadarshan, H. Simha, C. Bridges, A. Goel, T. Talon, A. Pedivellano, Y. Wei, F. Royer *et al.*, "Aarest autonomous assembly reconfigurable space telescope flight demonstrator," in *Proceedings of the 69th International Astronautical Congress (IAC)*. International Astronautical Federation (IAF), 2018.

[35] D. Gallagher, J. Bergstrom, J. Day, B. Martin, T. Reed, P. Spuhler, S. Streetman, and M. Tommeraasen, "Overview of the optical design and performance of the high resolution science imaging experiment (hirise)," in *Current Developments in Lens Design and Optical Engineering VI*, vol. 5874. International Society for Optics and Photonics, 2005, p. 58740K.

[36] T. Beck, B. Lüthi, G. Messina, D. Piazza, K. Seiferlin, and N. Thomas, "Thermal analysis of a reflective baffle designed for space applications," *Acta astronautica*, vol. 69, no. 5-6, pp. 323–334, 2011.

[37] ([Accessed: 28-02-2019]) Direct insertion to GEO. [Online]. Available: https://tinyurl.com/yydgqm6y

[38] W. J. Larson and J. R. Wertz, "Space mission analysis and design," Torrance, CA (United States); Microcosm, Inc., Tech. Rep., 1992.

[39] (internally distributed), "SSTL-42 spec sheet," SSTL, Guildford, UK, Tech. Rep., 1992.

[40] ([Accessed: 28-02-2019]) RRM site. [Online]. Available: https://sspd.gsfc.nasa.gov/robotic_refueling_mission.html

[41] S. Eckersley, C. Saunders, D. Lobb, G. Johnston, T. Baud, M. Sweeting, C. Underwood, C. Bridges, and R. Chen, "Future rendezvous and docking missions enabled by low-cost but safety compliant guidance navigation and control (gnc) architectures," in *Proceedings of The 15th Reinventing Space Conference*. British Interplanetary Society, 2017.

[42] Y. Ohkami and M. Oda, "Nasda's activities in space robotics," *EUROPEAN SPACE AGENCY-PUBLICATIONS-ESA SP*, vol. 440, pp. 11–18, 1999.

[43] L. Jackson, C. M. Saaj, A. Seddaoui, C. Whiting, and S. Eckersley, "The downsizing of a free-flying space robot," in *Annual Conference Towards Autonomous Robotic Systems*. Springer, 2019, pp. 480–483.

[44] ([Accessed: 28-02-2019]) SSTL media on DoT-4. [Online]. Available: https://www.sstl.co.uk/media-hub/latest-news/2018/sstl-announces-35kg-lunar-comms-mission-for-2021

[45] ([Accessed: 28-02-2019]) Intel realsense datasheet. [Online]. Available: https://www.mouser.co.uk/pdfdocs/Intel-RealSense-D400-Series-Datasheet_003.pdf

[46] ([Accessed: 28-02-2019]) ESPA user's guide. [Online]. Available: http://www.moog.com/content/dam/moog/literature/Space_Defense/spaceliterature/structures/Moog_ESPA_UsersGuide.pdf

[47] ([Accessed: 28-02-2019]) Spaceflight sherpa user's guide. [Online]. Available: http://www.spaceflight.com/wp-content/uploads/2015/05/SPUG-RevF.pdf

[48] T. Wekerle, J. B. Pessoa Filho, L. E. V. L. d. Costa, and L. G. Trabasso, "Status and trends of smallsats and their launch vehicles—an up-to-date review," *Journal of Aerospace Technology and Management*, vol. 9, no. 3, pp. 269–286, 2017.

[49] ([Accessed: 28-02-2019]) Firefly alpha user's guide. [Online]. Available: https://fireflyspace.com/wp-content/themes/firefly_aerospace/files/Firefly_Aerospace_Payload_User's_Guide.pdf

[50] ([Accessed: 28-02-2019]) Gaofen-4 online information. [Online]. Available: https://space.skyrocket.de/doc_sdat/gf-4.htm